the redistribution parameter in (21) cancels out. The distinction between a treatment using unscreened exchange, and one using screened exchange plus antiparallel correlation, is primarily semantic.

The apparently successful comparison of the theory developed in Sec. II with observed, interband optical absorption in the alkali metals can be interpreted in two ways. It is either an amusing coincidence, or it is a corroboration of the approximate treatment of exchange and correlation interactions given in Sec. III.[20]

[20] The alert reader will surmise that the strength of exchange and correlation interactions employed in this paper leads to an adiabatic instability of the electron gas. This observation would be a serious objection were it taken for granted that such an instability does not occur experimentally. Many observed anomalies in alkali metal properties can be explained provided an exchange instability has in fact altered the electronic ground state.

PHYSICAL REVIEW VOLUME 156, NUMBER 3 15 APRIL 1967

Excitons and the Absorption Edge in ZnSe

G. E. Hite,* D. T. F. Marple, M. Aven, and B. Segall
General Electric Research and Development Center, Schenectady, New York
(Received 6 October 1966)

The optical absorption threshold at about 2.7 eV, near the lowest-energy fundamental edge, was investigated for cubic ZnSe single crystals. Absorption spectra are reported for temperatures between 2 and 200°K, and absorption coefficients between 4 and 600 cm^{-1}. Although contributions associated with defects dominated the results in most crystals, intrinsic absorption could be observed for $T \gtrsim 60$°K in the purest available crystals. This intrinsic absorption results from longitudinal-optical-phonon-assisted creation of excitons, as is shown by the good agreement between the observed magnitude, the temperature, and photon-energy dependence, and the absorption calculated for this mechanism. The relevant exciton states involve electrons and holes from band extrema near the center of the Brillouin zone; when created without phonon assistance, excitons from these same extrema also give the relatively very intense "direct transition" absorption lines. No evidence is found that any band gap is smaller than that at the zone center.

I. INTRODUCTION

OPTICAL absorption spectra at the low-energy threshold for intrinsic electronic excitation have been studied for several elemental and compound semiconductors. Analysis of the temperature and energy dependence of these spectra have shown that in some instances, e.g., Ge and Si,[1] the absolute extrema in the conduction and valence bands are at widely separated points in the Brillouin zone, while in others, e.g., CdS[2,3] and CdTe,[4–6] these extrema are at or very near the same point. In the former case (Ge and Si), the absorption processes and corresponding band gap are called "indirect" and absorption is forbidden unless assisted by the simultaneous emission or absorption of one or more phonons of wave vector comparable to the differences between the wave vectors at the two band extrema.[7] In the latter case (CdS and CdTe), the processes and corresponding band gap are called "direct" and absorption is allowed without phonon participation. Absorption processes assisted by phonons of small or zero wave vector are also allowed for a direct gap.[3,6] These are of central importance in the discussion of the absorption spectra of the cubic (zinc-blende) modification of ZnSe presented in this paper.

Low-temperature optical studies of ZnSe[8] have already shown the existence of a very intense, narrow absorption band at an energy a few millielectron volts below the absorption continuum due to interband electronic transitions. This band was interpreted[8] as resulting from the creation of excitons associated with a direct gap, without phonon participation. Some other electrical[9] and optical[10] studies also suggested that the absolute conduction-band minimum was at the center of the Brillouin zone, and since the fluorescence emission spectra[11] (presumably due to bound excitons) were not significantly broadened by auto-ionization to a lower-energy continuum state, it was suggested[9] that the direct band gap associated with the excitons was, in fact, the smallest so that the absolute valence-band maximum was also at the center of the zone. In contrast, optical transmission studies had been reported

* Present address: Department of Physics, University of Illinois, Urbana, Illinois.

[1] T. P. McLean, in *Progress in Semiconductors*, edited by A. F. Gibson (John Wiley & Sons, Inc., New York, 1960), Vol. 5, pp. 55–101.
[2] D. G. Thomas and J. J. Hopfield, Phys. Rev. **116**, 573 (1959).
[3] D. G. Thomas, J. J. Hopfield, and M. Power, Phys. Rev. **119**, 570 (1960).
[4] D. G. Thomas, J. Appl. Phys. Suppl. **32**, 2298 (1961).
[5] D. T. F. Marple, Phys. Rev. **150**, 728 (1966) (referred to as I).
[6] B. Segall, Phys. Rev. **150**, 734 (1966) (referred to as II).
[7] See, e.g., R. J. Elliott, Phys. Rev. **108**, 1384 (1957).
[8] M. Aven, D. T. F. Marple, and B. Segall, J. Appl. Phys. Suppl. **32**, 2261 (1961).
[9] M. Aven and B. Segall, Phys. Rev. **130**, 81 (1963).
[10] D. T. F. Marple, J. Appl. Phys. **35**, 1879 (1964).
[11] D. C. Reynolds, L. S. Pedrotti, and O. W. Larson, J. Appl. Phys. Suppl. **32**, 2250 (1961).

TABLE I. Donor and acceptor concentrations of the ZnSe crystals used for optical studies.

Crystal No.	Source	Growing method	Regrowth	$N_D(10^{16}$ cm$^{-3})$	$N_A(10^{16}$ cm$^{-3})$
11	GE[a]	Epitaxial, vacuum	$3x$	17	16
35	Merck[a]	Self-nucleation, Ar	$1x$	1.1	0.75
42	E–P	Self-nucleation, Ar	$1x$	0.34	0.13

[a] The N_D and N_A values listed for crystals 11 and 35 are not the lowest obtained using GE or Merck material. Occasionally, and particularly when subjected to further purification, the crystals grown from GE ZnSe powder, for example, have shown N_A and N_D values as low as 1.8×10^{16} cm^{-3} and 0.5×10^{16} cm^{-3}, respectively.

to show that for ZnTe the smallest band gap is indirect,[12] and a $\mathbf{k}\cdot\mathbf{p}$ calculation[13] indicated that in ZnSe the absolute valence-band maximum was not at $\mathbf{k}=0$. Although this calculation has been recently corrected[14] and now supports the opposite conclusion, the earlier result was one of the reasons for undertaking this study of the absorption edge of ZnSe.

Intrinsic optical absorption in CdTe for energies in the minimum band-gap region has recently been measured[5] and interpreted[6] in studies which will henceforth be referred to as I and II, respectively. In I it was shown that the intrinsic absorption could not be satisfactorily understood in terms of an indirect band-gap model, and in II that it could be quantitatively accounted for with a direct band-gap model. Hence, it was decided that a similar study of ZnSe would be profitable.

While this work was in progress, results of two different studies of the interband Faraday effect were reported.[15,16] In both studies the results were shown to be consistent with the theoretical predictions for the rotation resulting from a direct band gap. However, it was not (and probably cannot be) shown that the data exclude the possibility of an indirect gap somewhat smaller than the direct gap. This is due to several complicating factors which make the interpretation of the rotation data more ambiguous than absorption-edge data.[17]

Our first absorption data showed that in ZnSe, as in other II-VI compounds, it was necessary to select and prepare the samples carefully in order to minimize "extrinsic" absorption due to native or foreign defects or to damaged surface layers. For $T\lesssim40$°K, the absorption was always partly or entirely due to such effects, but at higher temperatures intrinsic absorption dominated in the purest samples. The temperature and energy dependence of this intrinsic absorption was qualitatively similar to that reported in I for CdTe and could not be interpreted in terms of absorption processes at an indirect band gap. On the other hand, as discussed in II for CdTe, the absorption could be quantitatively shown to result from the creation of direct excitons (i.e., excitons associated with a direct band gap) together with the simultaneous absorption of longitudinal optical phonons. Thus these results confirm the earlier suggestions that the absolute extrema in both the conduction and valence bands are at the center of the Brillouin zone.

II. PREPARATION AND SOME PROPERTIES OF THE ZnSe BOULES

As already noted, absorption proved to be sensitive to the presence of crystalline defects. To study some of these effects ZnSe powders from three different suppliers, General Electric Company, Merck Chemical Corporation, and Eagle-Picher Corporation were used as starting materials and several crystal growing and purification techniques were employed. These materials and techniques are described in Appendix A. Optical studies were carried out on crystals grown from powder prepared by each of the three suppliers. One crystal (crystal No. 42) was found to be purer than the others (see below) by a substantial margin and spectra obtained with it also were the least influenced by defect-induced absorption. Spectra were obtained on samples from six other boules, and data for two of these (crystal No. 11 and crystal No. 35) are included in this report for comparison.

Table I gives the concentrations of electrically active donors N_D, and acceptors N_A, as obtained by analysis of Hall-effect data obtained on the crystals used for the optical studies. Because of its central position in this study, the impurity content of crystal No. 42 was extensively investigated after its purification with liquid Zn. (This purification procedure is described in Appendix A and discussed in Ref. 18.) Major chemical impurities found by mass spectroscopy[19] were C (15 ppm), N (8 ppm), O (62 ppm), and Fe (1.5 ppm). All other impurities, except for S, K, and Cu which were interfered

[12] A. C. Aten, C. Z. Van Doorn, and A. T. Vink, in *Proceedings of the International Conference on the Physics of Semiconductors, Exeter, 1962*, edited by A. C. Strickland (The Institute of Physics and The Physical Society, London, 1962), p. 696.
[13] M. Cardona, J. Phys. Chem. Solids **24**, 1543 (1963).
[14] M. Cardona, J. Phys. Chem. Solids **26**, 1351 (1965).
[15] M. Balkanski, E. Amzallag, and D. Langer, J. Phys. Chem. Solids **27**, 299 (1966).
[16] A. Ebina, T. Koda, and S. Shionoya, J. Phys. Chem. Solids **26**, 1497 (1965).
[17] These factors include: (a) Particularly for energies comparable to the band gap, the contributions to the wavelength dependence of the rotation from exciton states and from other valence and conduction bands may be significant. However they cannot readily be separated and were, in fact, neglected. (b) Calculation of the rotation involves integrations over parts of the Brillouin zone in which the usually employed parabolic-band approximation breaks down.
[18] M. Aven and H. H. Woodbury, Appl. Phys. Letters **1**, 53 (1962).
[19] Bell and Howell Research Center, Pasadena, California.

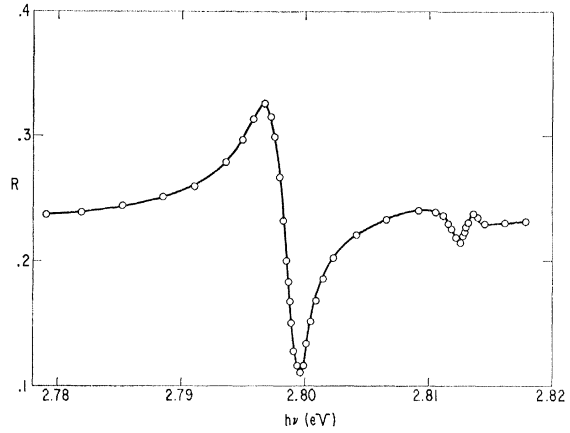

FIG. 1. Near-normal incidence reflectance of ZnSe crystal No. 44, zinc purified and chemically polished, shown as a function of photon energy for 2°K. Absolute reflectance values uncertain by about ±10%.

with by Zn and Se isotopes, were present in concentrations less than 1 ppm. Neutron activation analysis[20] for Cl, Br, and I showed no detectable amounts of these impurities (the detectability limits were 1.7, 0.9, and 0.7 ppm, for Cl, Br, and I, respectively).

III. PREPARATION OF THE OPTICAL SAMPLES AND MEASUREMENT TECHNIQUES

Optical samples were sawed from the crystal boules as parallel-sided plates. The two larger faces, each about $\frac{1}{2}$ cm^2 in area, were first ground and then mechanically polished with Linde "A" abrasive on a beeswax lap. Sample thicknesses ranged from 150 μ to 3 mm. As in other II-VI compounds (see, e.g., I), there is evidence that this polishing technique leaves an amorphous, damaged, surface layer. This damage was indicated by, e.g., the complete absence, at 80°K or below, of a sharp minimum in the reflectance associated with the creation of "direct" excitons; such a minimum is always observed in cleaved crystals. As shown in I, such a layer also significantly affects absorption as measured by transmission methods, and hence it was necessary to remove it chemically. Boiling concentrated NaOH has been used for this purpose,[8] but it is not very satisfactory for optical samples because it preferentially attacks grain boundaries and dislocations and causes severe pitting of some crystal faces. Much more satisfactory polishing action was obtained with a modified form of Ichimiya's etch[21] consisting of three parts saturated aqueous solution of $K_2Cr_2O_7$ and two parts concentrated H_2SO_4. The crystals were supported in a glass-mesh basket which allowed continuous agitation in 50 cc of this solution. Best results were obtained at temperatures between 95 and 100°C. At higher temperatures crystals were often partially covered with a dark gray, CS_2-insoluble deposit, while at lower temperatures there was noticeable preferential attack of grain boundaries. At 95 to 100°C, material was dissolved from each face at a rate of about 12 μ/min and after 3 to 4 min the samples were removed and rinsed in distilled water. They were then found to be coated with an orange film, probably amorphous Se, which was readily dissolved by CS_2 at room temperature. As a further precaution, the samples were immersed for 1 min in concentrated NaOH at 50°C, followed by a final rinse in distilled water. This chemical polishing procedure appears to have been adequate in removing distorted surface layers: Grazing-incidence-electron diffraction patterns from chemically polished samples showed that the surface was crystalline, the optical reflection structure due to the direct excitons was qualitatively the same as that seen in cleaved crystals, and concordant absorption data were obtained from samples of widely different thickness.

The techniques and apparatus used for the transmission measurements and the methods used to calculate the absorption from the data were essentially the same as those described in I. Because the peak absorption is so large, near-normal-incidence reflectance spectra were used to find the photon energies for maximum direct-transition absorption by ground-state excitons, E_{x1}. These spectra were obtained on zinc-fired crystal No. 42 at several temperatures between 2 and 200°K. For this purpose the Cary Model 14R spectrophotometer was modified by the addition of two diagonal

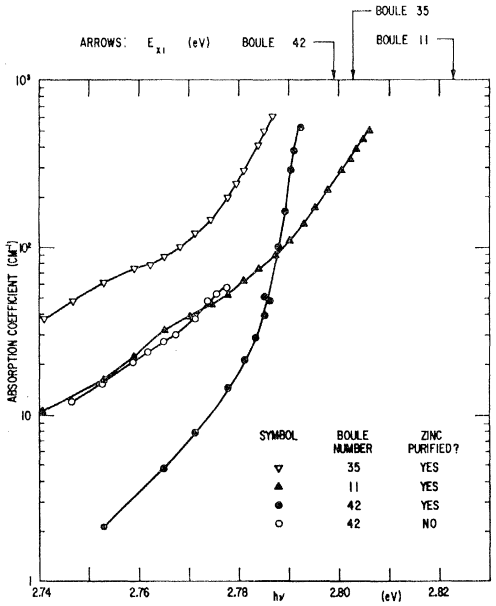

FIG. 2. Absorption coefficient α at 2°K, as a function of photon energy in ZnSe single crystal No. 42 before and after purification with liquid Zn, in crystal No. 35 after purification, and in crystal No. 11 after purification. Energies for maximum ground-state direct-transition exciton absorption E_{x1} are indicated by the vertical arrows.

[20] General Atomics, San Diego, California.

[21] T. Ichimiya, T. Niimi, K. Mizuma, O. Mikami, Y. Kamia, and K. Ono, *Solid State Physics in Electronics and Telecommunications* (Academic Press Inc., New York, 1960), p. 845.

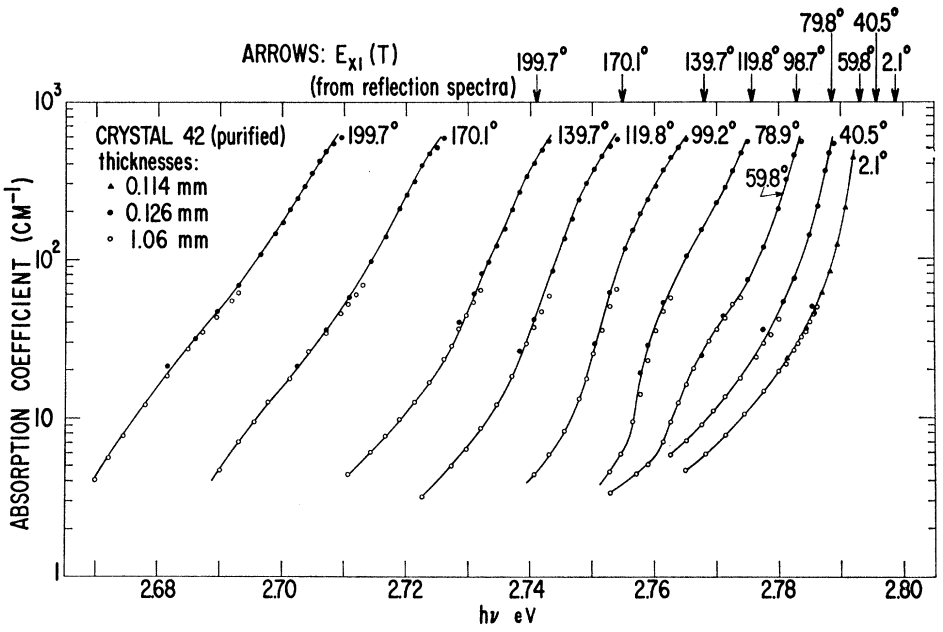

FIG. 3. Absorption coefficient α as a function of photon energy and temperature as observed in ZnSe single crystal No. 42 after purification with liquid Zn. Energies for maximum absorption by ground-state direct-transition excitons E_{x1} are indicated by vertical arrows for various temperatures.

mirrors and a compensating lens in both sample and reference beams. The maximum absorption was considered to occur at that energy where the reflectance was equal to the average of its values at the peak and the adjacent minimum. This rule gives a good approximation only for a relatively broad, weak absorption band with the classical Lorentzian line shape. However, all the results for E_{x1} so obtained agree within 1 meV with those found for the maximum in ϵ_2, the imaginary part of the dielectric constant, as obtained by Kramers-Kronig inversions of reflection spectra produced by a second similar crystal, No. 44. Figure 1 shows this spectrum as observed at 2°K with a Bausch and Lomb 2-m grating spectrometer equipped with a photoelectric scanner. Ground-state excitons cause the large peak-and-valley structure associated with the intense, narrow, absorption band, while the smaller structure is due to first-excited-state excitons.

IV. RESULTS AND DISCUSSION

A. Absorption Due to Chemical Impurities and Other Defects

Figure 2 shows the absorption coefficient at 2.1°K as a function of photon energy for samples from several different boules. The energies E_{x1} are indicated by vertical arrows. It is of interest to consider these results in relation to the data on sample purity in Table I and the accompanying text. As seen in the figure, E_{x1} is the smallest in the purest crystal (crystal 42) and largest in crystal 11, which also has the highest concentration of both donors and acceptors and of sulfur. Results with other crystals, not included here, show that this shift is associated primarily with the sulfur in solid solution[22] rather than the electrically active impurities. Figure 2 shows that for equal values of $E_{x1}-h\nu$ the absorption in crystal No. 11 is about the same as in No. 35, and for both it is larger, and with less abrupt energy dependence, than in crystal No. 42 after purification with liquid Zn. The extra absorption in crystals No. 11 and No. 35 is probably associated with crystalline defects, but the fact that it is the same in both (for equal values of $E_{x1}-h\nu$) suggests that it is not caused by the sulfur alone, nor by the electrically active impurities alone, since these are all considerably greater in crystal No. 11 than in crystal No. 35.

The importance of other chemical impurities such as noble metals is illustrated in Fig. 2 by the large decrease in absorption produced by purification of crystal 42 with liquid Zn. It seems likely that this absorption results from impurity-exciton complexes[23] since it lies much closer to the band gap than levels already reported for the isolated impurities.[24] The fact that Zn extraction reduces the absorption (rather than increasing it) also suggests that the absorption is not primarily due to uncompensated shallow donors. These would be expected to increase in concentration when the concentration of the Zn vacancies or Zn vacancy-donor complexes is reduced by the Zn-vapor firing. In any case, results obtained with crystal 42 after purification give an upper limit to the intrinsic absorption in the region near the

[22] S. Larach, R. E. Schrader, and C. F. Stocker, Phys. Rev. **108**, 587 (1957).

[23] M. Lampert, Phys. Rev. Letters **1**, 450 (1958); R. E. Halsted and M. Aven, *ibid.* **14**, 64 (1965).

[24] R. E. Halsted, M. Aven, and H. D. Coghill, J. Electrochem. Soc. **112**, 177 (1965).

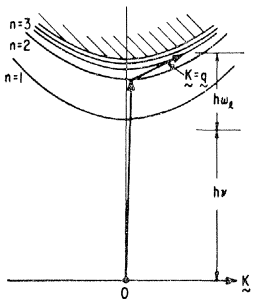

FIG. 4. Perturbation-theoretic representation of the creation of a "direct" exciton by optical absorption assisted by one phonon. The first step, in this representation, is the absorption of a photon which excites the crystal from the ground state ($E=0$, $\mathbf{K}=0$) to an intermediate state with $\mathbf{K}\approx 0$ on any one of the discrete exciton bands (the parabolas) or the continuum bands (the hatched area). In the second step the exciton is "scattered" by the absorption of an LO phonon of wave vector $\mathbf{q}$ to a final state with $\mathbf{K}\approx\mathbf{q}$ and energy $h\nu+\hbar\omega_l$. The scattering is represented by the smaller arrow.

exciton peak, and it is quite likely that the intrinsic absorption is actually significantly less than this limit.

B. Phonon-Assisted Exciton Absorption

Figure 3 shows the absorption in the Zn-purified crystal 42 as a function of photon energy $h\nu$ for several temperatures ranging from 2 to 198°K. These data are qualitatively similar to the corresponding results obtained for CdTe reported in Fig. 2 of I and, in general, the analysis of these data will follow that employed for CdTe. For the reasons already discussed in I, a satisfactory analysis in terms of indirect absorption processes is not possible. On the other hand, it will be shown that the intrinsic absorption (which dominates for $T\gtrsim 60$°K) results from the phonon-assisted creation of excitons.

TABLE II. Parameters used in calculation of phonon-assisted direct exciton absorption.

Parameter	Symbol	Value	Reference
Electron effective mass	m_e	$(0.17\pm0.025)m$	a
Hole effective mass	m_h	$0.75m$	b
Dielectric constant at E_{x1} in absence of exciton	ϵ'	8.1 ± 0.5	c
Static dielectric constant	ϵ_s	8.7 ± 0.1	d
High-frequency dielectric constant	ϵ_∞	5.60	e
Longitudinal-optical phonon energy	$\hbar\omega_l$	31.4×10^{-3} eV	e,f
Zero-frequency exciton polarizability	$4\pi\beta$	$(5.5\pm0.7)\times10^{-3}$	g
Exciton binding energy	B	21×10^{-3} eV	h
Ground-state energy of direct excitons	E_{x1}	2.80 eV	g

[a] D. T. F. Marple, J. Appl. Phys. 35, 1879 (1964).
[b] Selected to obtain best fit with data—see text.
[c] Reference 8 (taken from Fig. 4).
[d] S. Roberts and D. T. F. Marple (to be published) (from analysis of interference fringes observed in a single crystal in the 100–450-μ wavelength range at 4°K). A value of 9.1 at room temperature has been given by D. Berlincourt, H. Jaffe, and L. R. Shiozawa, Phys. Rev. 129, 1009 (1963).
[e] Low-temperature value estimated from room-temperature result [D. T. F. Marple, J. Appl. Phys. 35, 539 (1964)]. The stated value is the room-temperature value reduced by 5%, which was the reduction found in CdTe between 300 and 100°K [D. T. F. Marple (unpublished)], and in ϵ_s in ZnSe (see footnote d).
[f] R. E. Halsted, M. R. Lorenz, and B. Segall, J. Phys. Chem. Solids 22, 109 (1961).
[g] Obtained from normal-incidence reflectance spectra at 2.1°K shown in Fig. 1. The ground-state exciton absorption peak was obtained from the reflectance by the Kronig-Kramers inversion and this in turn was integrated to obtain $4\pi\beta$. The result is consistent with that reported in footnote c.
[h] Based on the separation of the peaks in ϵ_2 as seen in the Kramers-Kronig inversion of Fig. 1.

Figure 4 schematically represents the perturbation-theoretic description of the phonon-assisted exciton absorption. In the first step of this description, the annihilation of the photon with wave vector $\boldsymbol{\kappa}\approx 0$ creates a (Wannier) exciton in an intermediate state characterized by the exciton band index n_i and wave vector $\mathbf{K}_i=\boldsymbol{\kappa}\approx 0$. Upon the absorption of a longitudinal optic (LO) phonon with wave vector $\mathbf{q}$ and energy $\hbar\omega(\mathbf{q})$ in the second step, the exciton is "scattered" into the final state $n_f,\mathbf{K}_f\approx\mathbf{q}$. This process, which was first treated in studies of CdS[3] and ZnO,[25] was discussed in detail in II where significant corrections to the simplest results were calculated. In addition, the theory was extended in II to include the process involving the absorption of two phonons. As suggested in the first calculation[3,25] and as supported by the detailed considerations in II (Sec. V) the dominant electron-phonon coupling is the "polar" coupling to LO phonons with relatively small wave vector $\mathbf{q}$. Since to a good approximation $\hbar\omega_l(\mathbf{q})$ is independent of $\mathbf{q}$ for small $\mathbf{q}$, the phonon energy will be taken to be $\hbar\omega_l(0)=\hbar\omega_l$.

The results of the perturbation-theoretical calculations in II can be briefly outlined as follows. In the spectral range between E_{x1} and the threshold energy for the process involving one-phonon absorption, $E_{x1}-\hbar\omega_l$, the absorption is approximately given by $\alpha_{1\mathrm{ph}}(h\nu)$ while in the range between $E_{x1}-\hbar\omega_l$ and the threshold for the two-phonon process $E_{x1}-2\hbar\omega_l$ the absorption is given by $\alpha_{2\mathrm{ph}}(h\nu)$, where

$$\alpha_{1\mathrm{ph}}(h\nu)=N(\hbar\omega_l,T)\pi_1(h\nu)$$

and

$$\alpha_{2\mathrm{ph}}(h\nu)=N^2(\hbar\omega_l,T)\pi_2(h\nu)\,, \qquad (1)$$

with

$$N(\hbar\omega_l,T)=[\exp(\hbar\omega_l/KT)-1]^{-1}.$$

The Bose-Einstein function $N(\hbar\omega_l,T)$ in (1) determines the occupational probability of the LO phonons. As was shown earlier[3,25] and in II, the important energy dependent factors of $\pi_1(h\nu)$ and $\pi_2(h\nu)$ depend on the quantities E_{x1} and $h\nu$ only in the combination $E_{x1}-h\nu$. Since all of the other parameters (dielectric constants, effective masses, etc.) can for the present purposes be considered temperature-independent, the essential temperature dependence enters through $E_{x1}(T)$ and $N(\hbar\omega_l,T)$. The variation of the former translates the calculated absorption curves on the energy scale while the variation of the latter directly affects the magnitude. The only other relevant quantity with important temperature dependence is the exciton linebreadth Γ_n which is not incorporated into the perturbation cal-

[25] R. E. Dietz, D. G. Thomas, and J. J. Hopfield, J. Appl. Phys. Suppl. 32, 2281 (1961).

culations. The nonvanishing $\Gamma_n(T)$ proves to have significant effects[26] which will be discussed below.

Examination of Fig. 3 shows that particularly at the lower temperatures there are inflections in the energy dependence of the absorption. Maxima in slope are seen for example at $h\nu=2.751$, 2.758, and 2.761 eV for $T\simeq 99$, 79, and 60°K respectively. These are identified as the thresholds for absorption assisted by one LO phonon since for these temperatures $(E_{x1}-\hbar\omega_l)\simeq 2.752$, 2.758, and 2.762 eV, respectively, based on E_{x1} from Fig. 3 and $\hbar\omega_l$ from Table II. (This identification is strengthened when the background correction, discussed below, is included.) However, while (1) shows that $N(\hbar\omega_l,T)$ and hence the calculated $\alpha_{1\mathrm{ph}}$ decreases almost exponentially for $T<80$°K, Fig. 3 shows that for $T\lesssim 40$°K the observed absorption for a given value of $E_{x1}-h\nu$ is nearly independent of T, the temperature effect being almost entirely due to the shift in E_{x1}. This temperature-independent component of the absorption is believed to be largely "extrinsic" since it changes from crystal to crystal. It could result in part, for example, from transitions to localized (or "impurity") exciton states or transitions from the valence band to shallow donors (which can be viewed as transitions to ionized impurity excitons). Whatever its cause, it will be assumed that this extrinsic component is a background present at all temperatures and that the background-corrected absorption is

$$\alpha_c(T)=\alpha(T)-\alpha(2°\mathrm{K}), \tag{2}$$

where all quantities in (2) refer to the same value of $E_{x1}(T)-h\nu$. It is recognized that for several reasons α (2°K) is probably not an accurate measure of the extrinsic absorption at high temperatures. However, since the corrections are relatively very small at the higher temperatures ($T\gtrsim 120$°K), the procedure should be quite satisfactory for the intended purpose.

On account of the expected temperature dependence, α_c/N is plotted versus $E_{x1}(T)-h\nu$ in Fig. 5 for $E_{x1}(T)-h\nu<40$ meV and temperatures from 60 to 170°K. For $E_{x1}-h\nu<27$ meV, the data for all temperatures can be represented by one curve, within the possible errors in measurement of $E_{x1}(T)$ and α, as is expected from (1) for the absorption assisted by one LO phonon. However, it will be seen that as $E_{x1}-h\nu$ increases beyond 27 meV there is an increasing divergence between the results for α_c/N obtained at different temperatures. Equation (1) indicates that this divergence is at least partly due to the two-phonon process. In the simple approximation discussed above, this only contributes for $h\nu<E_{x1}-\hbar\omega_l$ although actually it makes some contribution above this energy. However, another effect leading to the noted spread in Fig. 5 is the appreciable

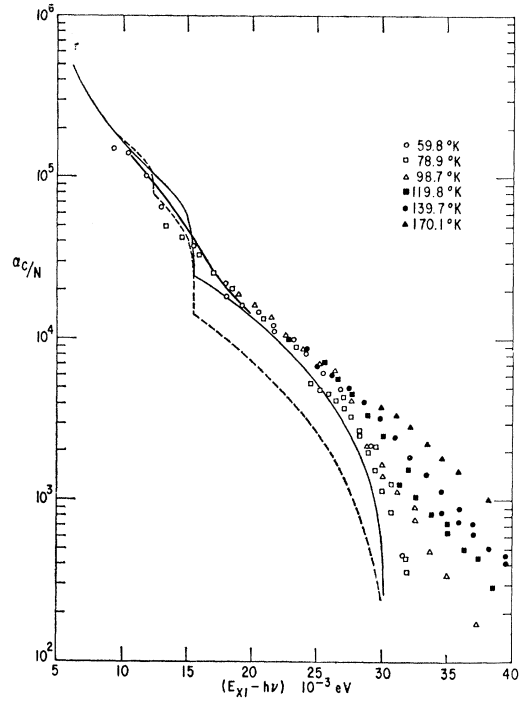

FIG. 5. Background-corrected absorption coefficient α_c divided by the phonon Bose-Einstein factor N, as a function of the energy difference $E_{x1}-h\nu$. Points are the data from Fig. 3 for temperatures from 60 to 170°K. The correction for background absorption is discussed in the text. Solid curve calculated by formulas given in the text and Appendix B for exciton absorption assisted by one phonon, with parameters given in Table II and $m_h=0.75$. Dashed curve calculated with the same parameters except $m_h=0.55$.

[26] B. Segall and D. T. F. Marple, Bull. Am. Phys. Soc. 11, 189 (1966).

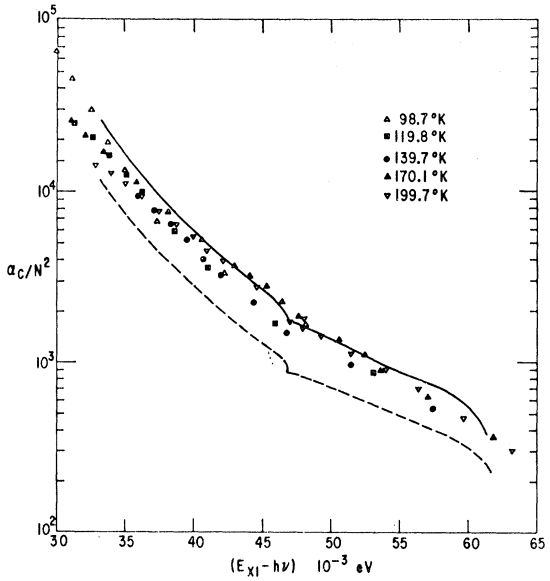

FIG. 6. Background-corrected absorption coefficient α_c divided by the square of the phonon Bose-Einstein factor N^2, as a function of the energy difference $E_{x1}-h\nu$. Points are the data from Fig. 3 for temperatures from 99 to 200°K. The correction for background absorption is discussed in the text. Solid curve calculated by formulas given in the text and Appendix B for exciton absorption assisted by two phonons, with parameters given in Table II and $m_h=0.75$. Dashed curve calculated with the same parameters except $m_h=0.55$.

exciton linewidth[26] at the higher temperatures. This has the effect of "smearing out" the threshold.

Figure 6 shows α_c/N^2 for $E_{x1}-h\nu$ in the range from 30 to 65 meV and includes data for temperatures from 99 to 200°K. In this case the fact that all the data lie (approximately) on a single curve supports the assertion that the absorption is assisted by two phonons. The data is scant for $E_{x1}-h\nu \lesssim 2\hbar\omega_l$ but the absence of any discernable threshold for this process presumably arises from causes similar to the analogous effect at the one-phonon threshold. An extrapolation of the data in Fig. 6 to $E_{x1}-h\nu<\hbar\omega_l$ and subtraction from α_c of the resulting N^2-dependent absorption removes much of the temperature dependence seen near the threshold in Fig. 5. However, because of the role of the level broadening and the uncertainty of the extrapolation in Fig. 6 near $E_{x1}-h\nu=\hbar\omega_l$ this is not a completely satisfactory procedure.

Figures 5 and 6 verify that α depends on T and $(E_{x1}-h\nu)$ as predicted by Eq. (1). The actual magnitude and detailed spectral dependence of α are given by π_1 and π_2 and will now be discussed. The basic approach and formulas for calculation of π_1 and π_2 are given in II and will not be repeated here. A tabulation of needed matrix elements which were not explicitly given in II and some notes on the computations are collected in Appendix B of this paper. Because of the increased direct-exciton linewidth, $E_{x1}-h\nu$ is least accurately known for data at the largest T, with the result that the positioning of the α_c/N^2 data is less accurately determined than that of α_c/N. Since $\pi_1(h\nu)$ can also be calculated more accurately than $\pi_2(h\nu)$ (which requires a third-order perturbation calculation), a comparison between π_1 and the data is more important and significant. $\pi_1(h\nu)$ can be expressed as

$$\pi_1(h\nu)=\alpha_1(h\nu)N^{-1}\Lambda^2[(1+G)^2+\sum_l \Delta_l]. \qquad (3)$$

Here $\alpha_1(h\nu)$ is the relatively simple result obtained when the intermediate and final states are restricted to the $n=1$ band and is given by Eq. (14) of II. Among others, α_1 contains factors that correspond to the electron–LO-phonon coupling constant and oscillator strength for an $n=1$ exciton. It thus essentially determines the magnitude of the absorption, while terms within the brace provide important correction factors that result from including states of n_{int} and $n_{\text{final}}>1$. The first term, $\Lambda^2(1+G)^2$, represents the correction associated with the $n>1$ intermediate bands. It is less than unity throughout the range, being smallest ($\sim\frac{1}{2}$) near $h\nu=E_{x1}-\hbar\omega_l$, and increasing monotonically to unity as $h\nu\rightarrow E_{x1}$. The term in $\sum_l\Delta_l$ (always >0) represents the correction from the $n>1$ final states which are consistent with over-all conservation of energy. In contrast with the intermediate states, for which only the $l=0$ bands contribute significantly, final states with all values of l must be considered. This correction increases steadily as $E_{x1}-h\nu$ decreases below the threshold for the $n=2$ exciton band.

In addition to E_{x1} and $\hbar\omega_l$, the parameters required to evaluate (3) are ϵ_∞, ϵ_s, and ϵ', the high- and low-frequency dielectric constants and the dielectric constant at $h\nu=E_{x1}$ with the exciton contribution omitted, m_e and m_h, the electron and hole effective masses, and $4\pi\beta$, the zero-frequency contribution from the $n=1$ exciton line to the polarizability (which is proportional to the oscillator strength). Table II lists values of these parameters as used in the computations along with relevant references. Of these, the least accurately known is m_h. The tabulated values of m_e, ϵ_s, and B, yield $m_h=0.4$ assuming "hydrogenic" binding, but any value between 0.2 and 0.8 is possible within the uncertainties in B and m_e. Because of this large range, m_h has been treated essentially as an adjustable parameter. It is to be noted that the valence band, which is believed[27] to be degenerate at $\mathbf{k}=0$ with symmetry Γ_8, is treated in the calculation as a simple (nondegenerate band). Thus m_h is some complicated average over the degenerate bands.

Figure 5 shows the calculated absorption as obtained with the tabulated parameters and the results in Appendix II. The solid curve corresponds to the results with $m_h=0.75$, while the dashed curve corresponds to those for $m_h=0.55$. The abrupt rise in these calculated curves at the $n=2$ threshold results from the final-state corrections and is clearly not reflected in the data. (The analogous thresholds for the $n=1$ state have already been noted for $T\lesssim 100$°K.) The absence of a distinct $n=2$ threshold results principally from the thermal broadening of the $n=2$ and higher exciton bands. This broadening was incorporated into the calculated absorption by the expedient of folding the $\Gamma_n=0$ result into a Lorentzian line-shape function with width, Γ_2, of 3 meV.[28] The result for $m_h=0.75$ is the heavier solid curve in Fig. 5, which is seen to agree satisfactorily with the data. It is noteworthy that the results from the folding prove to be insensitive to moderate changes in Γ_2, e.g., the result for $\Gamma_2=2$ or 4 meV is hardly distinguishable from that in Fig. 5.

Figure 5 shows that there is an appreciable increase in the slope of α_c/N as $E_{x1}-h\nu$ decreases below 14 meV (see especially the data for $T\approx 60$°K). To reproduce this increase in the calculated curve it is essential to include the final-state correction term $\sum_l\Gamma_l$, regardless of the choice of the parameters used. $\sum_l\Delta_l$ makes no contribution above 16 meV, but its inclusion more than doubles the calculated absorption at $E_{x1}-h\nu=10$ meV for $m_h=0.75$, for example.

Figure 5 shows that for $m_h=0.75$ the magnitude of the calculated absorption is in good quantitative agreement

[27] See, e.g., B. Segall, in *The Physics and Chemistry of II-VI Compounds*, edited by M. Aven and J. S. Prener (North-Holland Publishing Company, Amsterdam, 1966), Chap. 1; or Ref. 13.

[28] This width is a crude estimate based on reflection spectra for $T\cong 60$°K. For $T\geq 80$°K the structure due to the $n=2$ excitons is broadened to the extent that it can no longer be discerned.

with the data for $E_{x1}-h\nu<27$ meV, while for $m_h=0.5$ it is too small (by nearly a factor of 2 for $E_{x1}-h\nu<14$ meV). However, suitable changes in the other parameters within their uncertainties, particularly $4\pi\beta$, m_e, and B, would lead to an improved fit for the smaller value of m_h, so that the calculated curves should not be interpreted as decisively favoring the larger (average) hole mass over the smaller value.

The corresponding calculations for $\alpha_{2\mathrm{ph}}(h\nu)/N^2$, given by Eq. (25) of II, have been carried out with the same parameters as for $\alpha_{1\mathrm{ph}}$ and are shown as the solid and dashed curves in Fig. 6. Again, the result for $m_h=0.75$ agrees quite satisfactorily with the data while that for the smaller hole mass is somewhat too low. But for the reasons already given above, the significance in regard to the choice of m_h is not as clear as it appears in the figure.

It was already noted above that the threshold for the $n=1$ one-phonon-assisted absorption was increasingly blurred for $T>100$°K until at $T\approx200$°K, α increases almost exponentially (Uhrbach's rule). Both of these effects result from the thermal broadening of the ground-state exciton band.[6,26] As in the similar case of CdTe (see II) this was shown[26] for ZnSe by folding the calculated absorption curves of Figs. 5 and 6 with either Lorentzian or Gaussian ground-state exciton line-shape functions that had half-widths given by the Kramers-Kronig inversions of the reflection spectra. The resulting "blurred" absorption curves are in reasonable agreement with the data in the temperature range investigated (80 to 120°K). The results strongly suggest, as in the case of CdTe, that the exponential behavior observed at higher temperatures in ZnSe results from the phonon-assisted creation of *nonlocalized* excitons and not as usually suggested[29] from mechanisms involving *localized* (self-trapped) excitons very strongly coupled to the phonons.

V. SUMMARY

Optical absorption was measured at temperatures from 2 to 200°K for photon energies just below the direct exciton peak in ZnSe single crystals prepared from a variety of starting materials. The absorption, particularly for $T\lesssim40$°K, was found to be sensitive to crystalline perfection and the condition of the surfaces. The temperature and energy dependence of the absorption in the (chemically) purest crystals with suitably prepared surfaces was found to be primarily intrinsic for $\alpha>10$ cm^{-1} and $T\lesssim60$°K; for $T\gtrsim60$° the extrinsic absorption is independent of T except for the shift of the exciton-peak position.

The temperature dependence of the intrinsic absorption and the energies for the thresholds observed for $T<100$°K suggested that the intrinsic component was due to the creation of "direct" excitons assisted by the annihilation of one or more LO phonons. This explanation was confirmed by the quantitative agreement between the data and the magnitude and detailed energy dependence of the absorption as calculated using previously determined values of the direct exciton oscillator strength, dielectric constants, and electron effective mass. In these calculations an average hole mass was the only "adjustable" parameter and the value $m_h=0.75$, giving the best agreement with the data, lies within the (rather wide) limits set by the exciton spectrum. The effects of thermal broadening of the direct exciton states are discussed.

These results strongly support the view that ZnSe has a "direct" minimum band gap; no evidence was found for absorption by "indirect" transitions. Further, in conjunction with earlier optical and electrical studies, this work indicates that the conduction and valence band extrema are at (or very close to) the center of the Brillouin zone.

ACKNOWLEDGMENTS

The absorption calculations were programmed and run on the computer by E. L. Kreiger. G. P. Lloyd also assisted with the calculations and treatment of the data. The crystals were grown by W. Garwacki.

APPENDIX A: PREPARATION AND PURIFICATION OF THE ZnSe BOULES

The ZnSe powder obtained from the General Electric Chemical Products Plant (GE) was produced by a solid-state reaction between ZnS, ZnO, and Se. The starting materials used in this process are available in high-purity form, and the synthesis can be carried out at a relatively low temperature which minimizes contamination derived from contact with the reaction vessel. The disadvantage is an appreciable residual concentration of S($\sim10^3$ ppm in the grown crystals). As ZnS and ZnSe form a continuous series of solid solutions, this amount of S probably does not measurably influence properties like the carrier concentration, defect-center ionization energies, or mobility. However, changes in such parameters as the positions of narrow emission and absorption bands and the band gap are detectable. The ZnSe powder obtained from the Merck Company, the second supplier, was presumably synthesized by a variation of the method described by Benzing *et al.*[30] The starting product in this method is $ZnSeO_3$ (obtained by reacting Zn acetate with H_2SeO_3), which is reacted with hydrazine to form $ZnSe\cdot N_2H_4$. The hydrazino-selenide complex is decomposed to ZnSe by heating in inert atmosphere. The material is free from sulfur, but is often contaminated with pyrolysis product residues which have to be removed before crystals are

[29] See, e.g., R. S. Knox, in *Solid State Physics*, edited by F. Seitz and D. Turnbull (Academic Press Inc., New York, 1963), Suppl. 5, p. 155.

[30] W. C. Benzing, J. B. Conn, J. V. Magee, and E. J. Sheehan, J. Am. Chem. Soc. **80**, 2657 (1958).

grown. The ZnSe powder obtained from the Eagle-Picher Company, the third supplier, was prepared by a vapor-phase reaction between Zn and Se. Although some residual contamination is derived from the quartz reaction vessel, this material was the purest of the three suppliers.

The preparation of the GE and Merck ZnSe powder for crystal growth involved prefiring the material for 2 h at 500°C in flowing H_2 followed by 2 h at 800°C in flowing Ar. All materials were sintered in Ar at 1000°C for 2 h prior to insertion in crystal-growing tubes. The crystals were synthesized by two different modifications of the vapor-phase growth method. The first process, described by Piper and Polich[31] (see also Baker *et al.*[32]), was carried out in 1 atm Ar and relied on self-nucleation of the vapor-transported material in the drawn-out tip of the growing tube. The second process, described by Shiozawa *et al.*,[33] used sublimation in vacuum onto a single-crystal seed. In both methods the tube filled with partially sintered powder was pushed through a temperature gradient, and the powder sublimed from the hot to the cold end of the tube. As applied to ZnSe, an essential feature of these methods was to place and move the growing tube in the temperature gradient so as to effect first a backwards growth of the sintered powder charge and then to resublime the resulting polycrystalline boule forward into the front portion of the tube. The forward sublimation was carried out until about 75% of the backward-grown boule was resublimed. This regrowth effected a significant concentration of impurities into the remaining 25% of the back-diffused portion and a corresponding purification of the forward-diffused material. Two further steps in purification, multiple regrowing and solvent extraction[18] were performed on some of the crystals. In multiple regrowing, a crystal grown from sintered powder was itself used as starting material for another boule, the process being repeated two or three times. The solvent extraction involved firing the crystals for 20 to 60 h in molten Zn at 850°C. This has been shown[18] to be particularly effective in removing the noble-metal impurities Cu and Ag.

APPENDIX B

As noted in the text (Sec. IV.B), the basic expressions required for the computations were given in II and will not be repeated here. In this Appendix, the matrix elements, which were not specifically given in II, will be tabulated and some aspects of the computations will be discussed. References to the specific equations in II will be indicated by, for example, Eq. (II-14).

[31] W. W. Piper and S. J. Polich, J. Appl. Phys. **32**, 1278 (1961).
[32] L. C. Greene, D. C. Reynolds, S. J. Czyzak, and W. M. Baker, J. Chem. Phys. **29**, 1375 (1958).
[33] L. R. Shiozawa, J. M. Jost, G. P. Chotkevys, S. S. Devlin, J. L. Barrett, and T. R. Slyker, Sixth Quarterly Report Contract No. AF-33(657)-7399, Electronics Division, Clevite Corporation, 1963 (unpublished).

TABLE III. Constants $\gamma_{n,l}$ and functions $\beta_{n,l}(p)$ needed in evaluating matrix elements of U [Eq. (A2)].

n	l	$\gamma_{n,l}$	$\beta_{n,l}(p)$
1	0	1	$[1+(p/2)^2]^{-2}$
2	0	1.1174	$(2p/3)^2[1+(2p/3)^2]^{-3}$
3	0	0.3248	$(3p/4)^2[1+3(3p/4)^2][1+(3p/4)^2]^{-4}$
4	0	0.16384	$(4p/5)^2[1+22(4p/5)^2/5+5(4p/5)^4][1+(4p/5)^2]^{-5}$
2	1	1.1174	$(2p/3)[1+(2p/3)^2]^{-3}$
3	1	0.3978	$(3p/4)[1+3(3p/4)^2][1+(3p/4)^2]^{-4}$
4	1	0.21981	$(4p/5)[1+22(4p/5)^2/5+5(4p/5)^4][1+(4p/5)^2]^{-5}$
3	2	0.4593	$(3p/4)^2[1+(3p/4)^2]^{-4}$
4	2	0.3560	$(3p/4)^2[1+(3p/4)^2]^{-4}$ [a]
4	3	0.11723	$(4p/5)^3[1+(4p/5)^2]^{-5}$

[a] Approximate.

In the computation of $\pi_1(h\nu)$ [or $\alpha_{1\mathrm{ph}}(h\nu)$] of Eq. (1) it is necessary to compute $\alpha_1(h\nu)$, the result obtained when the intermediate- and final-state bands are restricted to $n=1$. $\alpha_1(h\nu)$ is given by Eqs. (II-14) and (II-12). The correction factors in (1) are obtained from Eqs. (II-16) and (II-19). Specifically,

$$\Lambda=(\langle E_{xn}\rangle-E_{x1})/(\langle E_{xn}\rangle-h\nu) \tag{A1}$$

and $(1+G)$ is given by the summation within the absolute value sign of Eq. (II-16). In the computations of G for ZnSe, terms with $n>3$ were neglected. $\sum_l \Delta_l$ represents the correction for all final states (consistent with energy conservation) for $n=1$ intermediate states.

It is convenient to write the necessary matrix elements as:

$$i^{-l}\langle 1,0|U|n,l\rangle=\gamma_{n,l}[\beta_{n,l}(p_{h,n})+(-)^{l+1}\beta_{n,l}(p_{e,n})], \tag{A2}$$

where $\gamma_{n,l}$ and $\beta_{n,l}(p)$ are given in Table III (for $n\leq 4$ and $l\leq 3$), and to note that

$$|\langle 1,0|U|n,l\rangle|=|\langle n,l|U|1,0\rangle|. \tag{A3}$$

In (A2) the momentum variables are

$$p_{e,n}=(m_e/m_h)^{1/2}\xi_n^{1/2} \quad \text{and} \quad p_{h,n}=(m_h/m_e)^{1/2}\xi_n^{1/2}, \tag{A4}$$

where

$$\xi_n=[\hbar\omega_l+h\nu-E_{xn}]B^{-1}, \tag{A5}$$

with B the exciton binding energy.

It is convenient to write

$$\sum_l \Delta_l=\sum_l \Delta_l{}^d+\sum_l \Delta_l{}^c, \tag{A6}$$

where the first term on the right is the contribution from the discrete states and the second term that from energetically allowable continuum states. Equations (A3)–(A5) are applicable for the continuum states (labeled by $\mathbf{k}$, the wave vector for the relative motion) when the discrete eigenvalues $E_{x,n}=E_G-B/n^2$ are replaced by those from the continuum $E_{x,\mathbf{k}}=E_G+Bk^2a^2$.

The expression for the first term in (A6) is

$$\Delta_l{}^d=\xi_1{}^{1/2}|\langle 1,0|U|1,0\rangle|^{-2}\times\sum_{n>1}{}'\,\xi_n{}^{-1/2}|\langle 1,0|U|n,l\rangle|^2, \quad \text{(A7)}$$

while that for $\Delta_l{}^e$ is obtained by the replacement indicated above and

$$\sum_{n>1}{}'\rightarrow\frac{1}{2}\int_0^{\xi_1-1}d\xi_k.$$

The contribution to $\xi_1{}^{-1/2}|\langle 1,0|U|1,0\rangle|^2\Delta_l{}^d$ from $n\geq 5$ is approximated by

$$l=0:\quad B_3Q_1{}^2(p_{\bar{n}})+B_5Q_1(p_{\bar{n}})Q_2(p_{\bar{n}}), \quad \text{(A8)}$$

$$l=1:\quad 15.57A_3(D-0.7399F)^2+65.61A_5(F-D)(D-0.7399F), \quad \text{(A9)}$$

$$l=2:\quad 11.53C[\beta_{3,2}(p_{\mathrm{h},\bar{n}})-\beta_{3,2}(p_{e,\bar{n}})]^2. \quad \text{(A10)}$$

In these expressions the matrix elements were evaluated for fixed $p_{e,\bar{n}}$ and $p_{h,\bar{n}}$ with $\bar{n}=7$. The quantities in (A8)–(A10) are defined as

$$A_m=(\xi_1-1)^{-1/2}\sum_{n=5}^{\infty}n^{-m}(1-n^{-2})\times[1+(\xi_1-1)^{-1}n^{-2}]^{-1/2}, \quad \text{(A11)}$$

$$B_m=(\xi_1-1)^{-1/2}\sum_{n=5}^{\infty}n^{-m}[1+(\xi_1-1)^{-1}n^{-2}]^{-1/2}, \quad \text{(A12)}$$

$$C=(\xi_1-1)^{-1/2}\sum_{n=5}^{\infty}n^{-3}(1-4n^{-2})(1-n^{-2})\times[1+(\xi_1-1)^{-1}n^{-2}]^{-1/2}, \quad \text{(A13)}$$

$$Q_1(p)=S_1(p_h)-S_1(p_e), \quad \text{(A14)}$$

$$2Q_2=S_3(p_h)-S_3(p_e)-[S_4(p_h)-S_4(p_e)]/3, \quad \text{(A15)}$$

where $S_k(p)$ is defined in Eq. (II-18);

$$D=\beta_{3,1}(p_{h,\bar{n}})-\beta_{3,1}(p_{e,\bar{n}}), \quad \text{(A16)}$$

$$F=\beta_{2,1}(p_{h,\bar{n}})-\beta_{2,1}(p_{e,\bar{n}}). \quad \text{(A17)}$$

TABLE IV. Approximations to $\gamma_{n,l}$ and $\beta_{k,l}$ of Eq. (A2) for continuum states.

l	γ_l	$\beta_{k,l}(p)$
0	1	$S_1(p)-k^2[S_3(p)-S_4(p)/3]/4$
1	3.946	$(1+k^2)^{1/2}\{[\beta_{3,1}(p)-0.7399\beta_{2,1}(p)]-2.1070k^2[\beta_{2,1}(p)-\beta_{3,1}(p)]\}$
2	7.594	$(1/5+k^2)^{1/2}\beta_{3,2}(p)$
3	14.424	$(1+14k^2)^{1/2}\beta_{4,3}(p)$

For the continuum states the matrix elements in the form (A2) are approximated by the forms given in Table IV.

For the ZnSe computations, the contribution to $\sum_l\Delta_l$ from the sum of terms with $l\geq 3$ is estimated to be about 1% of that from the combined $l=0$, 1, and 2 terms and thus is neglected.

The expression for $\pi_2(h\nu)$, and hence $\alpha_{2\mathrm{ph}}(h\nu)$ is given in Eqs. (II-23) and (II-25). Except for the matrix element,

$$\langle 1,0|U(2za^{-1})U(2z'a^{-1})|1,0\rangle=(1+m_e\sigma/m_h)^{-2}+(1+m_h\sigma/m_e)^{-2}-(1+m_ez'^2/M+m_hz^2/M-\sigma)^{-2}-(1+m_ez^2/M+m_hz'^2/M-\sigma)^{-2},$$

where

$$\sigma=(4B)^{-1}[h\nu+2\hbar\omega_l-E_{x1}]$$

and

$$M=m_e+m_h;$$

the remaining matrix elements required to evaluate π_2 are given above. The same approximations discussed and used in II were employed here. The contribution of discrete final states with $n>4$ was found to be very small and was neglected. The contribution of the final states in the continuum was calculated in the manner indicated above with the limits on the integral being zero and $\xi_1-1+\hbar\omega_l/B$. For these computations all final states with $l\leq 3$ were included with the $l=3$ contribution being only a few percent of the total.